Numerical Study of Debris Flight in a Tornado-like Vortex

Huo, Ryan; Hemida, Hassan; Sterling, Mark

[Link to publication on Research at Birmingham portal](#)

Manuscript Details

Manuscript number	YJFLS_2020_84_R1
Title	Numerical Study of Debris Flight in a Tornado-like Vortex
Article type	Research Paper

Abstract

This paper presents the numerical study on the flight behaviour of spherical compact debris in a tornado-like wind field. The tornado-like vortex corresponding to a swirl ratio of 0.7 was generated using Large-eddy Simulation and the trajectories of 2250 individual debris particles placed in the flow were computed using Lagrangian-particle tracking. The debris corresponded to five groups (A, B1, B2, B3 and C) based on the value of the Tachikawa number (K) which ranged between 0.6 and 2.5. An analysis of the simulated flow field revealed that the tornado-like vortex consisted of two main features - a core at the centre with low velocity (~0.25m/s) which was surrounded by thick vortex wall composed of high velocity magnitudes (~9.4m/s). Updraft flows were observed around the core of the vortex and as a result, debris positioned around the core radius region were found to be 24% more likely to become wind-borne than debris positioned at the vortex wall region. Three groups of debris (B1, B2 and B3) with varying mass and density were studied for the aerodynamic similarity by retaining the fixed value of K=1.2; all three debris groups exhibited the propensity to travel with similar flight characteristics. An analysis of the data pertaining to the fight behaviour of the three debris group (A, B1 and C) with varying K revealed that the low mass debris group A (K=2.5) had the highest propensity to become wind-borne and was more likely to travel for the longest time with considerable variability observed in individual debris trajectories. However, somewhat counterintuitively, the high mass debris group C (K=0.6) were found to have the furthest impact range despite their short flight duration; this was due the high mass debris being ejected out of the vortex with greater inertia, while debris with a lower mass had a tendency to be trapped in the flow that circulates around the vortex core.

Keywords	CFD; flying Debris; tornado-like vortex; large eddy simulation
Corresponding Author	Shuan Huo
Corresponding Author's Institution	University of Birmingham
Order of Authors	Shuan Huo, Hassan Hemida, Mark Sterling

Submission Files Included in this PDF

File Name [File Type]

Cover letter.doc [Cover Letter]

Responses to reviewers comments.docx [Response to Reviewers]

Numerical Study of Debris in Tornado-like Vortex (clean).docx [Manuscript File]

declaration-of-competing-interests.docx [Conflict of Interest]

CRediT author statement.docx [Author Statement]

Numerical Study of Debris in Tornado-like Vortex (tracked changes).docx [Supplementary Material]

Submission Files Not Included in this PDF

File Name [File Type]

Figure 1.png [Figure]

Figure 2.png [Figure]

Figure 3.png [Figure]

Figure 4.png [Figure]

Figure 5.png [Figure]

Figure 6.png [Figure]

Figure 7.png [Figure]

Figure 8.png [Figure]

Figure 9.png [Figure]

Figure 10.png [Figure]

Figure 11.png [Figure]

Figure 12.png [Figure]

Figure 13.png [Figure]

Figure 14.png [Figure]

Figure 15.png [Figure]

Figure 16.png [Figure]

To view all the submission files, including those not included in the PDF, click on the manuscript title on your EVISE Homepage, then click 'Download zip file'.

Research Data Related to this Submission

There are no linked research data sets for this submission. The following reason is given:
Data will be made available on request

Mr Shuan Huo

University of Birmingham

School of Engineering

University of Birmingham

Edgbaston

Birmingham

B15 2TT

UK

9th February 2020

Dear Professor Langre,

We wish to submit a full-length research article entitled "Numerical Study on Debris Flight in a Tornado-like Vortex" by Shuan Huo, Hassan Hemida and Mark Sterling for possible publication in the Journal of Fluids and Structures.

We confirm that this work is original and has not been published elsewhere, nor is it currently under consideration for publication elsewhere.

Please address all correspondence concerning this manuscript to me at srh629@bham.ac.uk.

Thank you for your consideration of this manuscript. I look forward to hearing from you in due course when the review process has been completed.

Yours sincerely,

Shuan Huo
Ph.D Student
Department of Civil Engineering
School of Engineering
University of Birmingham

The authors would like to thank the reviewers for their comments which have given us an opportunity to reflect on the paper and make adjustments. In what follows we address and embrace the comments by both reviewers. Two versions of the paper are provided – a clean version and a tracked changes version indicating where the text has been altered. For the benefit of the reviewers, changes are listed below with new text highlighted using a yellow background.

Reviewer 1

This paper presents a numerical study of debris flight in a tornado-like flow. The conditions for the initialization of the flight and the impacts of the flow and debris characteristics on the flight trajectory are comprehensively investigated. Part of the numerical results are compared to previously published experimental results. Since there have only been few studies of debris flights in tornadoes, the outcomes presented in this paper can be valuable for subsequent studies. However, the reviewer does recommend that two major problems and a number of minor problems be addressed before the paper can be published in Journal of Fluids and Structures.

Major problems:

1. The reviewer believe that the paper should be more willing to acknowledge the limitations of the numerical study instead of liberally brushing these limitations and in many places simply saying the numerical results are good even when such an assessment is not warranted.

Examples include but are not limited to:

(1) The paper suggests that the numerical and experimental results presented in Figure 6 agree very well and that there are only minor differences around the core region. However, a simple inspection of this figure can reveal quite significant differences between the numerical and experimental profiles, even in regions away from the core. Moreover, the paper simply attributes the differences to the uncertainty of the experiments. This, to the reviewer, is a little cavalier, as computational fluid dynamics based simulations are to date far from perfect.

The fully authors agree and acknowledge that in places they make have not been as reflective as they should have been, for that we apologise.

New text has been added to **line 193 - 196** as follows:

…figure 2. Whilst every effort has been made to accurately reproduce the physical simulator their will inevitably be small differences introduced due to the meshing process. It is difficult to quantity the impact of these differences, but in what follows it is assumed that beyond a certain mesh resolution their effects are negligible (see section 3).

The following change has been made to **lines 291 - 300**

Overall, the predicted velocity field matches that given by the physical results. However, both the numerical and physical simulations are not without their limitations: accurately specifying inflow boundary conditions are crucial for LES yet fraught potentially with difficulties (Yang, 2015), as very specific information on turbulence is required to reproduce identical inflows, e.g., turbulence intensity, stochastically varying turbulent length scales, and power spectrums of turbulent etc. The effects of SGS modelling is also considered to be a potential source of uncertainty since SGS motions inevitably requires unrealistically fine

cells at all regions even locations far away from the vortex structure. Notwithstanding these limitations, the numerical results presented in the paper are within the range of experimental uncertainty and considered suitable for the purposes of this work

Page 14, line 360 - 361 now read:

Both the numerical and experimental results correspond well (considering the uncertainty associated with the results) at the location $r/r_c=1$ with the overlapping trajectory path of approximately 78%; while at the location $r/r_c=2$, the overlapping region was lower at approximately 61%

And **page 20, line 500** now read:

Acknowledging the uncertainty associated with the data, the numerical simulations agree well with previous experimental research and provide a greater insight into the flow field.

(2) In the discussion regarding Figure 9, apparent differences again exist between the numerical and experimental results. However, the paper states that the numerical and experimental results "correspond well" and again attributes the differences only to the "the larger variation in the trajectory paths from the experiments, caused by the turbulent fluctuation in the local field." Shouldn't the numerical simulation faithfully reproduce the turbulent fluctuation in the local field? How well does the numerically simulated turbulence compare with the turbulence measured in the experiments?

The authors agree (in part), but note that given the uncertainties now acknowledged a faithful reproduction of the physical data in all of the domain is unlikely. In addition, we note that turbulent intensities were not compared to the experiments due to the absence of the latter in the papers (associated with the difficulties of obtaining reliable measurements) (Gillmeier et al., 2017; Bourriez et al., 2017). Thus, we have adjusted the text as follows **(page 15, line 386 - 395)**:

In general, the prediction of debris trajectories corresponds well for both the numerical simulation and experiments results; however, it should be pointed out that debris were assumed to be one-way coupled and the motion of debris were also assumed with no rotation in a highly swirling flow, which may result in some difference in overall trajectories between numerical and physical simulation. We also note the lack of turbulence data associated with the physical measurements results in an uncertainty of the flow simulation in this region. Notwithstanding this the numerical simulation are consistent with the physical data and able to capture the entire flight duration from initialization to the impact on the ground. Furthermore, the numerical simulations provide a better understanding of the impact distribution and extend the results of the physical simulation.

2. The paper suggests flight initializations occur mainly in regions where updrafts are present. Can this be due to the oversimplification of the problem? First, the study assumes that the debris does not rotate. This can be very different from reality, especially in the presence of a flow field that is very three dimensional and inhomogeneous, and lead to oversimplification of the interaction between the fluid and the debris. Also, how well does the numerical model simulate the interaction between the

debris and the flow even with the assumption? The reviewer understands the challenges involved and is not suggesting that the paper should not be published given the limitations. However, the paper should at least acknowledge these limitations.

> The authors appreciate this question and it is something that they have long pondered. Inspection of the debris corresponding to the physical data suggests that this may not be the case due to the relative size of the debris and the curvature of the streamlines – we acknowledge that the resolution of the physical data is limited in this regard (and probably would not stand up to rigorous peer review) so we cannot be certain, but this is our current working assumption. We also note that this is a working assumption which has been embraced by others (Holmes, 2004; Baker, 2007; Wills et al., 2002) who have concluded that the trajectories and velocities can be reasonably predicted by only considering the action of the drag force and gravitational force acting on the debris. However, we also acknowledge that this area of research is very much in its infancy. On reflection, we agree that this should be acknowledged in the paper and as such have introduced new text as follows **(page 20, line 529 - 534)**:

> It is worth noting that current study only considers the flow field of the vortex at S=0.7. Different swirl ratios have the potential to result in different flow characteristics and those would affect the overall behaviour of wind-borne trajectory. Further, the flight characteristics of debris were assumed with no rotation, which might be considered less realistic in a highly swirling vortex flow field when the rotation of debris generates lift, which would lead to a different interaction between the fluid and debris.

> We have also highlighted the lack of rotation of the particles in a number of other locations in the text, but have not listed these below (e.g., see **line 202, line 389, and line 532**).

Less significant problems:

1. The paper provides two inconsistent definitions of the aspect ratio: one from line 115 to line 116, and the other according to equation (2).

> This was an oversight on our part which has now been corrected. **(page 4, line 130 - 133)**:

$$S = \frac{tan\theta}{2a} \qquad [1]$$

> where θ is the guide vanes angles and a is the aspect ratio, defined as:

$$a = \frac{2h_2}{D_3} \qquad [2]$$

> The definition of the aspect ratio is based on the physical dimensions of the simulator; the ratio between the diameter of the exhaust outlet (D_3) and the height of the inlet (h_2).

2. Lines 156-157: The descriptions of the axes are not correct.

> The descriptions of the axes have been adjusted **(page 5, line 161 to 163)**:

where the xy plane represents the horizontal plane while z axis represents the axis perpendicular to the horizontal plane.

3. What are the shapes of the debris? Are those spheres since only the diameters are given?

The reviewer is correct; the geometric configurations of the debris are spheres. Additional descriptions have been added. (**line 13 and line 201**):

This paper presents the numerical study on the flight behaviour of spherical compact debris in a tornado-like wind field.

And

Each individual debris was assumed to be a three dimensional spherical compact

Reviewer 2

The rationale behind the LES simulation for tornadic like vortex flow simulation was well explained, carried out with OpenFOAM. The CFD simulation domain was modelled after the Birmingham simulator, with experimental results from Gillmeier used as validation. Mesh convergence study was carried out to determine the flow structure sensitivity.

Airborne debris simulations were based on experimental tests performed at the University of Birmingham and showed good agreement. Conclusions drawn on the flight time as a function of Tachikawa number (K) and debris impact location were unique and useful contributions to the field of tornado research. The conclusions made are sensible based on the fluid mechanics of the tornado vortex.

Overall the paper is worthy of publication, but there are minor comments that should be addressed before the paper is published. In summary:

1. No explanation was given as to why a swirl ratio of 0.7 was selected for the study. I'm assuming that it was due to limited experimental data made available to them, but I would think that this parameter would have very important implications on the resulting trajectory and flight times or the airborne debris.

> The reviewer is correct on the selection of the swirl ratio and their assumption. We have undertaken both physical and numerical simulations for another swirl ratio but chose not to include the results in order to keep the paper a reasonable length. We adjusted the text as follows to acknowledge the reviewer's point (**page 20, line 529 - 531**):

> It is worth noting that current study only considers the flow field of the vortex at S=0.7. Different swirl ratios have the potential to result in different flow characteristics and those would affect the overall behaviour of wind-borne trajectory.

2. The aspect ratio definition based on the physical dimensions of the test apparatus which may lead to a different aspect ratio if the tornadic fluid structure instead. Gairola and Bitsuamlak 2019 (JWEIA) has modelled three different tornado testing chambers (UWO, IOWA, TEXAS TECH) and discussed this aspect ratio issue, can you comment how the aspect ratio defined using the Birmingham testing apparatus fits with others?

> The authors are incredibly comforted by the fact that the reviewer has raised this point since it proves that others are starting to appreciate this fact as well. For the last few years this is an issue that we have also been raising at many international conferences, is what Gillmeier based her PhD thesis on and is formally stated in a peer review journal (Gillmeier et al. 2019). It is thus with great pleasure that we add the following text (**page 20, lines 533 – 536 and page 4, line 133 - 136**):

> …which would lead to a different interaction between the fluid and debris. It is also worth noting that this work has simulated the flow assuming one single definition of aspect ratio, but as indicated by Gillmeier et al. (2019) and Gairola and Bitsuamlak (2019), this may be an important area which has hitherto largely been neglected.

By the way, this reviewer noticed notable tornado related papers missing in the reference including the one mentioned here.

> We have included a number of references and would happily include more if we have missed a notable reference which is relevant to the current work. However, there has been a trend of late (particularly in a certain journal) to include papers for the sake of name checking certain authors. We are not averse to adding more references of direct relevance, but the reviewer would need to tell us what notable papers we are missing.

3. Within the literature review, it was stated that Ward-type tornado simulators were unable to provide reliable and accurate insights into the vortex flow structure. I believe that this is a misleading comment, but rather the Ward simulators were limited by their size and design to reproduce some characteristics of tornado flow (such as translating effects), but were effective in investigating other characteristics.

> The following text has now been added (**page 2, lines 46 - 48**):

> …vortex and provided an alternative to study tornado flows. However, Ward's simulators were limited by their size unable to reproduce some vortex characteristics due to the design.

4. Abstract: tornado like "vortex" is missing

> This was an oversight on our part which has now been corrected.

5. The low percentage of windborne debris were attributed to ignoring the translation effects of the tornado, can you add a context how much velocity are we missing from the translation that affects the result. (see line 306-309).

> The context of translating speed have been provided in the revised manuscript as requested. (**page 11, line 322 to 327**)

> The low percentage of windborne debris were not too surprising as this study focuses only on the wind-borne behaviour in a stationary tornado, where the translation effects of the tornado were ignored. However, it is worth nothing that the translational movement of a naturally occurring tornado could potentially result in higher percentage of debris becoming wind-borne; several researches (Kosiba et al., 2014; Matsui et al., 2008; Phuc et al., 2012) have been carried out where the translating speed of tornado ranges from 0.05 U_T to 0.7 U_T.

Numerical Study of Debris Flight in a Tornado-like Vortex

Shuan Huo*[1], Hassan Hemida[2], Mark Sterling[3]

Department of Civil Engineering, School of Engineering, University of Birmingham, Birmingham, United Kingdom

1) srh629@bham.ac.uk
2) h.hemida@bham.ac.uk
3) m.sterling@bham.ac.uk

Abstract

This paper presents the numerical study on the flight behaviour of spherical compact debris in a tornado-like wind field. The tornado-like vortex corresponding to a swirl ratio of 0.7 was generated using Large-eddy Simulation and the trajectories of 2250 individual debris particles placed in the flow were computed using Lagrangian-particle tracking. The debris corresponded to five groups (A, B1, B2, B3 and C) based on the value of the Tachikawa number (K) which ranged between 0.6 and 2.5. An analysis of the simulated flow field revealed that the tornado-like vortex consisted of two main features - a core at the centre with low velocity (~0.25m/s) which was surrounded by thick vortex wall composed of high velocity magnitudes (~9.4m/s). Updraft flows were observed around the core of the vortex and as a result, debris positioned around the core radius region were found to be 24% more likely to become wind-borne than debris positioned at the vortex wall region. Three groups of debris (B1, B2 and B3) with varying mass and density were studied for the aerodynamic similarity by retaining the fixed value of K=1.2; all three debris groups exhibited the propensity to travel with similar flight characteristics. An analysis of the data pertaining to the fight behaviour of the three debris group (A, B1 and C) with varying K revealed that the low mass debris group A (K=2.5) had the highest propensity to become wind-borne and was more likely to travel for the longest time with considerable variability observed in individual debris trajectories. However, somewhat counterintuitively, the high mass debris group C (K=0.6) were found to have the furthest impact range despite their short flight duration; this was due the high mass debris being ejected out of the vortex with greater inertia, while debris with a lower mass had a tendency to be trapped in the flow that circulates around the vortex core.

1. INTRODUCTION

Tornadoes are perhaps one of the most destructive weather phenomena due to their potentially violent and unpredictability nature. The wind speeds of a tornado can reach up to 450 kilometres per hour and can cause severe damage to civil structures and loss of lives. In March 2019, a tornado struck the Lee County in Alabama (USA) and caused catastrophic damage around the region: it was reported that the tornado was classed as an EF4 with wind speeds reaching 270 kilometres per hour (Darrow, 2019) and claimed the lives of more than 23 people. Tornadoes are complex phenomena and despite their frequent occurrence, surprisingly little is known about the flow structure. Due to the violent nature and unpredictable path of tornadoes, details of the tornado flow field using full scaled methods have, to date, proved to be rather elusive; therefore, recourse is often made through physical and numerical modelling. The earliest systematic experiment for generating laboratory-scaled tornado-like vortices can perhaps be attributed to Ward (1972). Ward developed a laboratory simulator with an exhaust fan at the top to provide updraft flow and vanes at the ground to generate angular momentum. This approach enabled the reproduction of tornado-like flow from a single-celled vortex

46 into a multi-celled vortex and provided an alternative to study tornado flows. However, Ward's
47 simulators were limited by their size unable to reproduce some vortex characteristics due to the
48 design. Therefore, an increasing number of studies have been conducted in order to numerically
49 simulate such flow.

50 Recent numerical studies have been conducted extensively to study the flow fields of tornado-like
51 vortices. Howells et al. (1988) and Nolan and Farrell (1999) used the axisymmetric Navier-Stokes
52 equations in cylindrical coordinates to examine the flow structure of a tornado-like vortex. Lewellen
53 et al. (1999) conducted Large-eddy Simulation (LES) to examine the interaction between the
54 generated vortex and the surface roughness. Unsteady Reynolds-Averaged Navier-Stokes (URANS)
55 model for the numerical simulation were performed by Hangan and Kim (2006) to reproduce tornado-
56 like vortices. They concluded that the core of the tornado was the most difficult region to properly
57 reproduce. Lewellen and Lewellen (2007) employed a LES turbulence model to study the effects of
58 swirl ratio (a parameter which measures the strength of a circulation relative to the updraft flow) on
59 vortex structure and translation speed. Kuai et al. (2008) conducted numerical research on full scale
60 and laboratory simulated tornadoes using the k-ε turbulence model and verified the ability of
61 numerical methods to capture the flow fields of the tornadoes. Hangan and Kim (2008) conducted
62 simulations using an URANS model to reproduce tornadoes at different swirl ratios, and discovered
63 that a high swirl ratio corresponded with full scale data from the Spencer tornado observed by
64 Alexander and Wurman (2005). Ishihara et al. (2011) compared the flow fields of two different types
65 of vortices and validated the results with the laboratory experiments. Natarajan (2011) numerically
66 simulated different stages of tornadoes and confirmed the findings from earlier physical simulations
67 is the primary governing parameter of a vortex. Research undertaken by Ishihara and Liu (2014)
68 conducted an in-depth study of a tornado-like vortex during touch down stage with detailed analysis
69 of the flow field; while Liu and Ishihara (2015) further investigated the stages of tornado-like vortices
70 in order to capture of characteristics of the evolution of different vortex stage. The excellent research
71 conducted by the aforementioned researchers and others provides an insight to tornado flows and its
72 mechanism; however, the definition of the swirl ratio from these studies varies from one to another,
73 therefore, detailed discussions on the definition of swirl ratio employed in this study were discussed
74 in section 2.2.

75 Another key factor that contributes to the tornado induced damage is flying debris. Everyday objects
76 can become damaging projectiles when subject to a tornado, and individuals have been affected
77 considerably by debris which become windborne as a result of a tornado (Harms, 2019). Numerous
78 research on flying debris have been undertaken since the pioneering works of Tachikawa (1983), which
79 proposed a dimensionless parameter, K, which describes the ratio between the inertial forces of the
80 flow to the weight of the debris. Wills et al. (2002) categorized debris based on their respective
81 damage performance with light, medium or heavy weight missiles; other identification based on the
82 geometrical structure can further categorize the debris into compact type (3D), plate type (2D) and
83 rod type (1D). Further work on the trajectories of compact type (3D) spherical debris in strong winds
84 was conducted by Holmes (2004) and English (2005). Baker (2007) also generalized the equations of
85 motion for debris flight in dimensionless form for compact and sheet-like debris. Furthermore, plate-
86 like (2D) debris (Tachikawa, 1983; Wang and Letchford, 2003; Holmes et al., 2004) and rod-like (1D)
87 debris (Lin et al., 2007; Richards et al., 2008) under different wind conditions have also been studied
88 extensively, but none of these studies were carried out under tornado-like flow conditions. Recently,
89 several investigations on debris flight in tornadoes have been conducted; Maruyama (2011) simulated
90 a tornado-like vortex using large eddy simulations with the statistical distribution of debris velocities.
91 Bourriez et al. (2017) studied the flight paths of debris in laboratory controlled conditions. Research
92 undertaken by Baker and Sterling (2017) provided an analytical model for the velocity and pressure

93 fields of tornadoes as well as the prediction of debris trajectories within the tornado. While these
94 studies provide a great insight to the flow fields and trajectories, there is a lack of detailed analysis on
95 flying debris in tornadoes. Hence, the objective of the present work was to investigate the behaviour
96 of flying debris in a tornado-like wind field. The tornado-like vortex was simulated using LES. The flow
97 fields of the vortex were analysed and the characteristics features were presented. Trajectories of five
98 debris groups with varying Tachikawa number were computed and the flight data were analysed.

99 The paper is organized as follows: Section 2 describes the procedure adopted and the numerical
100 details relating to this. Section 3 outlines the three dimensional flow field, characteristics and
101 mechanisms of the simulated tornado-like vortex. The detailed analysis of debris flight in tornado wind
102 field were discussed in section 4. Appropriate conclusions are given in section 5.

2. METHODOLOGY

2.1 DESCRPTION OF PHYSICAL SIMULATOR

105 The model used in the current research was based on the University of Birmingham Tornado Vortex
106 Generator (UoB-TVG), shown in figure 1. A series of physical simulations were undertaken by Gillmeier
107 et al. (2017) and were used as validation for the numerical flow field simulated in the current paper.
108 The UoB-TVG was a large-scale Ward-type vortex generator based on the design of Ward's simulator
109 (Ward, 1972) with exhaust fans placed at the top of the convection chamber that were used to
110 generate an updraft flow. Situated below the convection chamber was the convergence chamber,
111 designed to draw air inwards with a series of guide vanes mounted at the edge of convergence
112 chamber. Angular momentum was obtained by setting the guide vanes to different angles, thus
113 generating different vortex structures. The convection chamber has the height, h_1 of 2m and diameter,
114 D_1 of 3.1m and convergence chamber with the height, h_2 of 1m and diameter, D_2 of 3.6m with thirty
115 guide vanes mounted around the edges of the convergence chamber. An exhaust outlet with
116 diameter, D_3 of 1m was situated at the top of the convection chamber. The ratio between updraft
117 diameter and the height of the convergence chamber was defined as the aspect ratio, a. The velocity
118 at the inlet (U_∞) was 0.66m/s, which was computed based on the measured total outflow rate (Q) of
119 7.38 m³/s at the exhaust outlet. The velocity measurements of the flow field were made 100Hz using
120 the Cobra Probe (Watkins et al., 2002) which was mounted in the simulator.
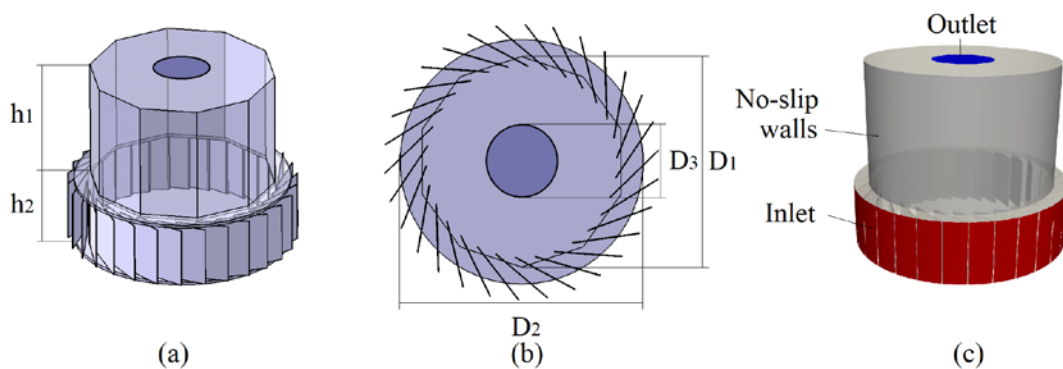
Figure 1: (a) Geometry of the University of Birmingham Tornado Vortex Generator (b) Dimensions of the convergence chamber (c) Computational domain and boundary conditions.

2.2 SWIRL RATIO

125 Whilst there are some variations for the definitions of swirl ratio in most laboratory studies (Monji,
126 1985, Mishra et al., 2008, Matsui and Tamura, 2009, Tari et al., 2010 and Gillmeier et al., 2017) and
127 numerical studies (Wilson and Rotunno, 1986, and Ishihara et al., 2011 and Ishihara and Liu, 2014),

128 the swirl ratio has generally been defined as the measure of intensity of the circulation of a vortex,
129 while also describing the evolution of the stages of a tornado; from single-celled to multi-celled vortex.
130 The swirl ratio, S used in the current research has been defined as:

$$S = \frac{tan\theta}{2a} \tag{1}$$

131 where θ is the guide vanes angles and a is the aspect ratio, defined as:

$$a = \frac{2h_2}{D_3} \tag{2}$$

132 The definition of the aspect ratio is based on the physical dimensions of the simulator; the ratio
133 between the diameter of the exhaust outlet (D_3) and the height of the inlet (h_2). The UoB-TVG has a
134 fixed aspect ratio of 2, while other large-scale tornado vortex simulators have adjustable aspect ratios
135 such as the WindEEE dome (Refan and Hangan, 2018) with aspect ratio of 0.35 to 1, VorTECH (Tang et
136 al., 2017) of 0.5 to 1 and ISU Tornado simulator (Gairola and Bitsuamlak, 2019) of 1.09 to 5.46.

2.3 NUMERICAL DETAILS

138 The Large-eddy simulation approach employed in the current research was first proposed by
139 Smagorinsky (1963); the LES uses sufficiently small grid resolution to directly compute the larger
140 eddies in a turbulent flow, while the smaller unresolved scales of the turbulence were filtered and
141 modelled via the sub-grid scale (SGS). Studies by Natarajan (2011), Maruyama (2011), Ishihara et al.
142 (2011) and Ishihara and Liu (2014) found that the vortex core contains complicated turbulent flows
143 and thus ideally suited to an LES. The open source CFD program OpenFOAM (OpenFOAM, 2019) was
144 used to perform the LES with the assumption that the flow was incompressible and Newtonian in
145 nature. The continuity and momentum equations were filtered as follows in order to obtain the
146 governing equations:

$$\frac{\partial \overline{U}_i}{\partial x_i} = 0 \tag{3}$$

$$\frac{\partial \overline{U}_i}{\partial t} + \frac{\partial \overline{U}_i \partial \overline{U}_j}{\partial x_j} = -\frac{\partial \overline{P}}{\partial x_i} + 2\frac{\partial}{\partial x_j}(v + v_{sgs})\bar{S}_{ij} \tag{4}$$

147 where U is the velocity field, t is the time and v is the kinematic viscosity. The spatial filtering operation
148 for the LES is denoted by the bar over the physical quantities. The pressure (P) and filtered strain rate
149 tensor ($\bar{S}_{ij}$) are expressed as:

$$\overline{P} = \frac{\bar{p}}{p} + \frac{(\overline{U_iU_j} - \overline{U}_i\overline{U}_j)}{3} \tag{5}$$

$$\bar{S}_{ij} = \frac{1}{2}\left(\frac{\partial \overline{U}_j}{\partial x_i} + \frac{\partial \overline{U}_i}{\partial x_j}\right) \tag{6}$$

150 The Smagorinsky model (Smagorinsky, 1963), was used to model the eddy viscosity under the effects
151 sub-grid scale, v_{sgs} with the eddy viscosity coefficient as:

$$v_{sgs} = (C_s f_d \Delta)^2 \sqrt{2\bar{S}_{ij}\bar{S}_{ij}} \qquad [7]$$

152 where f_d is the damping function, Δ is the length scale of the SGS turbulence and C_s is the model
153 coefficient, set to 0.1. The Van Driest type damping function (Van Driest, 1956) was employed in this
154 study to calculate f_d and is expressed as:

$$f_d = 1 - exp\left(\frac{-y^+}{25}\right) \qquad [8]$$

155 where y^+ is the non-dimensional distance to the wall, depicted as the relationship between friction
156 velocity and kinematic viscosity.

2.4 COMPUTATIONAL DOMAIN AND BOUNDARY CONDITIONS

158 The computational domain was created based on the configurations of the UoB-TVG, which was
159 geometrically similar to the study by Gillmeier et al. (2017) as illustrated in figure 1. The convection
160 chamber was simplified to a cylinder configuration for the convenience of grid generation. A cartesian
161 coordinate system has been adopted for the generation of the computational domain, where the *xy*
162 plane represents the horizontal plane while *z* axis represents the axis perpendicular to the horizontal
163 plane. The flow enters the convergence chamber with a uniform velocity of U_∞=0.66 m/s. The exhaust
164 outlet was set with pressure outlet with the free stream pressure, $P_\infty=0$. A no-slip boundary condition
165 was applied to the ground, surface walls of the guide vanes and the walls of the convection region.
166 The results presented in this study were normalized using the characteristic parameters of the vortex:
167 the maximum tangential velocity (U_T), the radius of the core (r_c) and time per revolution of the vortex
168 (t_r). The method of determining the location of maximum tangential velocity and the radius of the core
169 are presented in section 3.2, while the time taken for the vortex to complete a single revolution is
170 defined as:

$$t_r = \frac{2\pi r_T}{U_T} \qquad [9]$$

171 where r_T is the radial distance of the maximum tangential velocity. The pressure coefficient, C_P, is a
172 non-dimensional parameter defined as:

$$C_p = \frac{P - P_\infty}{0.5\,\rho_a U_T{}^2} \qquad [10]$$

173 and ρ_a is the density of the air. The simulation was initialised with the inlet velocity, U_∞. A second
174 order implicit backward scheme was used to approximate the time discretization. The gradients were
175 discretized with the second order central differencing scheme and the implicit PISO solver was used.
176 (OpenFOAM, 2019). A constant time-step *of Δt= 5x10^{-4}* s was used throughout the entire transient
177 simulation; this time-step was chosen to maintain the Courant-Friedrichs-Lewy number (Courant et
178 al., 1928) at the value less than 1 at every time step. The averaging of pressure and velocity were
179 implemented when the vortex flow was fully developed, this was conducted by monitoring the
180 residuals of each turbulent equation for convergence which ensured that the statistics did not change
181 with time. Time time-averaged results were obtained by averaging the actual simulation time of 30
182 seconds, which is equivalent to 300 vortex revolutions.

183   **2.5 MESHING**

184   ICEM-CFD (ICEM, 2012) mesh generator package was used to generate quadrilateral structured mesh.
185   In order to resolve the boundary layer around the viscous sub-layers, 20 layers of mesh were created
186   with the wall-adjacent spatial unit of z^+=1. Due to the axisymmetric structure of the tornado-like
187   vortex, a clustered mesh with high density was adopted at the centre of the convergence chamber
188   within the radius of 0.6 m from the centre, resulting in x^+ and $y^+≈10$ in the tangential and radial
189   directions. Hyperbolic stretching was used to generate the remaining meshes to ensure smooth
190   transition. The mesh resolution around the guide vane regions in the convergence chamber were
191   adjusted for the generation of three different mesh resolutions - coarse, medium and fine mesh with
192   4 million, 7 million and 9 million cells respectively. The configuration of the generated mesh is shown
193   in figure 2. Whilst every effort has been made to accurately reproduce the physical simulator there
194   will inevitably be small differences introduced due to the meshing process. It is difficult to quantity
195   the impact of these differences, but in what follows it is assumed that beyond a certain mesh
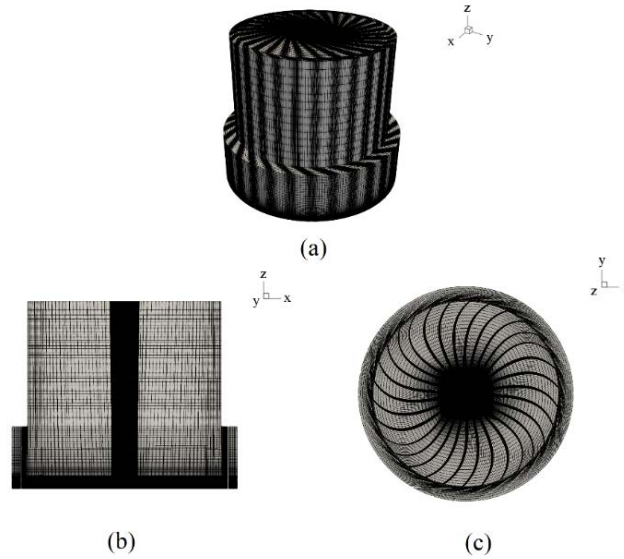196   resolution their effects are negligible (see section 3).

197

198   *Figure 2: Mesh of the computational domain: (a) Isometric view (b) Side view) (c) Top view.*

199   **2.6 COMPUTATION FOR FLYING DEBRIS**

200   The three-dimensional motion of the debris in the tornado-like vortex was numerically computed.
201   Each individual debris was assumed to be a three dimensional spherical compact object which did not
202   undergo rotation. The Tachikawa number (Tachikawa, 1983) used in the current research is defined
203   as:

$$K = \frac{\rho_a U_\infty^2 d^2}{2 m_d g}$$

[11]

204   where ρ_a is the density of the air, U_∞ is the inlet velocity, d is the diameter of the debris, m_d is the
205   mass of the debris and g is the acceleration due to gravity. The Tachikawa number K, describes the
206   ratio between the aerodynamic forces to the gravitational force, therefore, debris with lower mass
207   will have higher value of K and are in theory, prone to fly higher and further. Properties of the debris
208   considered in the current study were shown in table 1.

209

Table 1: Properties of the debris groups

Debris group	K	Diameter (m)	Density (kg/m³)	Mass (kg)
A	2.5	0.00075	28.1	6×10^{-9}
B1	1.2	0.0015	28.1	50×10^{-9}
B2	1.2	0.00075	56.2	12×10^{-9}
B3	1.2	0.00037	112.4	3×10^{-9}
C	0.6	0.003	28.1	397×10^{-9}

210 The trajectories of the debris were computed using the transient solver
211 icoUncoupledKinematicParcelFoam (OpenFOAM, 2019), where the motion was solved by considering
212 the particle equilibrium using the Lagrangian frame of reference on the established flow field. Since
213 the size of the largest debris considered (debris group C) was ~10^8 times smaller than the convergence
214 chamber, the effects of debris on the flow were considered to be negligible. Hence, a one-way
215 coupling was assumed to be sufficient, where debris were treated as point mass and generalized by:

$$\frac{ds_d}{dt} = U_d \tag{12}$$

$$m_d \frac{dU_d}{dt} = F_{total} \tag{13}$$

216 where s_d is the spatial position of the debris, U_d is the debris velocity, and F_{total} as the sum of all forces.
217 The relevant forces acting on the particle were:

$$F_{total} = F_D + F_G \tag{14}$$

218 where F_D is the drag force and F_G is the gravitational force. These forces represent the dominant forces
219 acting of the debris, while other forces were neglected. The drag force is expressed as:

$$F_D = \frac{3}{4} \frac{\rho_a}{\rho_d} \frac{m_d}{d} \cdot C_D (U - U_d)|U - U_d| \tag{15}$$

220 where U is the velocity of the local flow field, and C_D is the spherical drag coefficient that is computed
221 based on the debris Reynolds number (Putnam, 1961) as:

$$C_D = \begin{cases} \frac{24}{Re_d}(1 + \frac{1}{6}Re_d^{\frac{2}{3}}), & Re_d \leq 1000 \\ 0.424, & Re_d > 1000 \end{cases} \tag{16}$$

222

$$Re_d = \frac{\rho_a U d}{\mu_a} \tag{17}$$

223 where μ_a is the viscosity of air. Each debris group was simulated for 50 time instances in the flow. At
224 each time step, 9 debris were placed at different radial positions on the ground to be initialized by the
225 flow, at 0m, 0.0275m, 0.55m, 0.0825m, 0.11m, 0.165m, 0.22m, 0.275m and 0.33m. A total of 2250
226 debris were released in the flow field.

3. RESULTS FOR THE TORNADO-LIKE VORTEX

3.1. ASSESMENT OF NUMERICAL ACCURACY

In order to investigate the impact of grid resolution on the numerical results, computations were conducted on three mesh resolutions- coarse, medium and fine meshes. The velocity components U_t, U_r and U_v represents the tangential, radial and vertical velocities respectively. Due to the axis-symmetrical structure of the vortex, horizontal positions from the centre were expressed using the radial distance, r. Figure 3 shows the comparison of vertical distribution of time averaged tangential velocity extracted from different locations, r=0.1, 0.15, 0.2 and 0.25m. At all radial positions, the coarse, medium and fine meshes show similar trends with respect to the vertical distribution of the tangential velocity, with the medium and fine meshes both predicted similar results. The maximum tangential velocities obtained from the three meshes are 11.7, 12.4 and 12.5 m/s for coarse, medium and fine meshes, respectively.
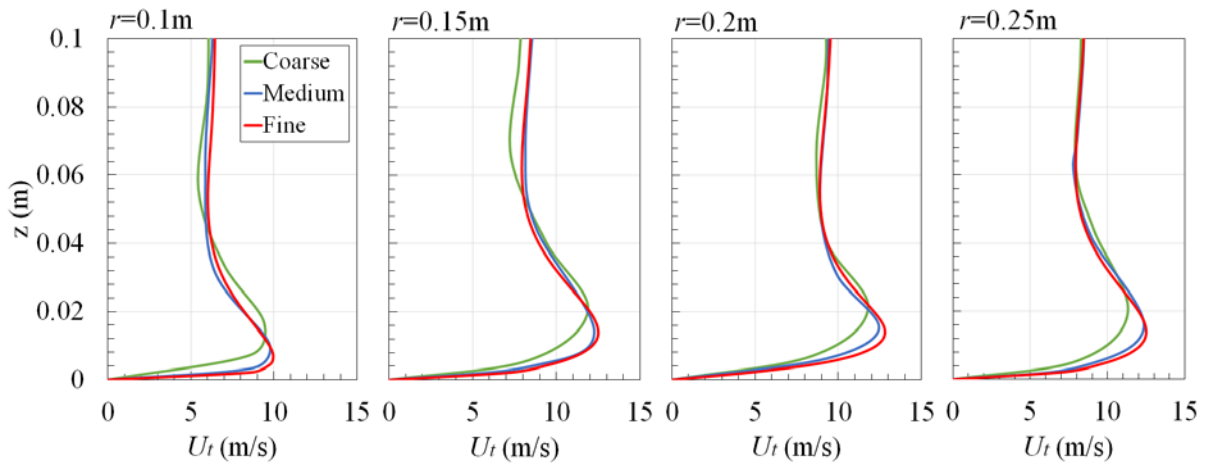

Figure 3: Vertical profiles of time averaged tangential velocity at the position r/r_c= 1, 1.5, 2 and 2.5.
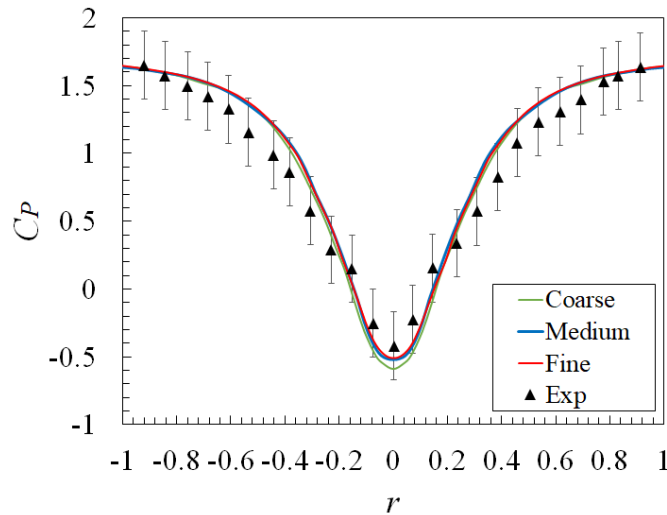

Figure 4: Distribution of time averaged pressure coefficient on the ground surface in comparison with experimental data Gillmeier et al. (2017).

The experimental results of Gillmeier et al. (2017) were used as a comparison for the numerical simulation. It is worth noting that experimental velocity and pressure data have an uncertainty of ± 2% and ± 0.5%. Figure 4 illustrates the agreement between the numerical simulations and experimental data in terms of surface pressure coefficient. For all meshes it can be observed that the

248 data from LES agrees well in terms of magnitude and trend with the experimental data. (A comparison
249 using the velocity measurements is presented later in section 3.2 and shows a similar level of
250 agreement with the medium mesh.)

3.2 FLOW FIELD

252 The results from the numerical simulation of a tornado-like vortex with the swirl ratio of 0.7 are
253 presented in this section. The flow features of the vortex structure were analysed and the method of
254 determining the radius of the core and vortex wall thickness are discussed. Figure 5 illustrates the
255 contours of instantaneous velocity magnitude and the vectors of averaged radial and vertical velocity,
256 where U_{mag} denotes the velocity magnitude of the flow field. The tornado-like vortex consists of two
257 main features, a vortex core and thick vortex walls. The core is situated at the centre of the vortex
258 while the wall surrounds the core and gives an outline to the structure of the vortex. The vortex was
259 observed to exhibit a very minor and random wandering motion where the core shifts at the maximum
260 distance of approximately r/r_c=0.18 from the centre axis. Based on the velocity vectors, the centre of
261 the vortex consists of downwards flow - a region of inflow was observed towards the centre, and then
262 redirects towards the vertical direction. The radial distance in which separates the upwards and
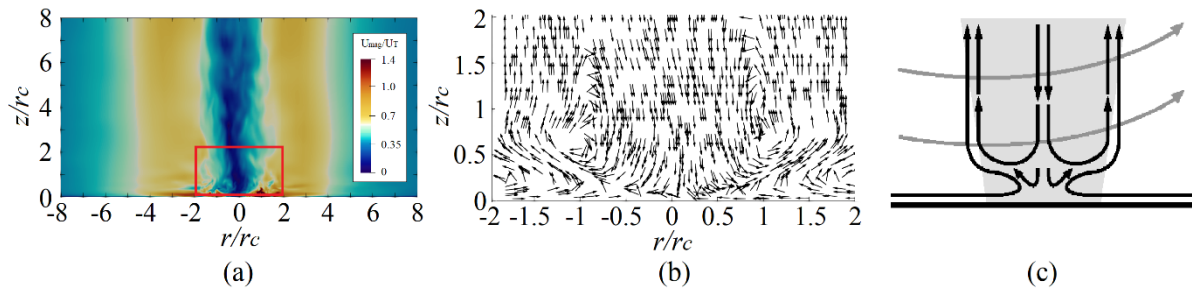263 downwards flow was identified as the core radius.

264

Figure 5: (a) Contours of instantaneous velocity magnitude of tornado-like vortex (b) Averaged radial and vertical velocity vector of the regions in the red box (c) Sketch of the tornado-like vortex to illustrate the flow structure.
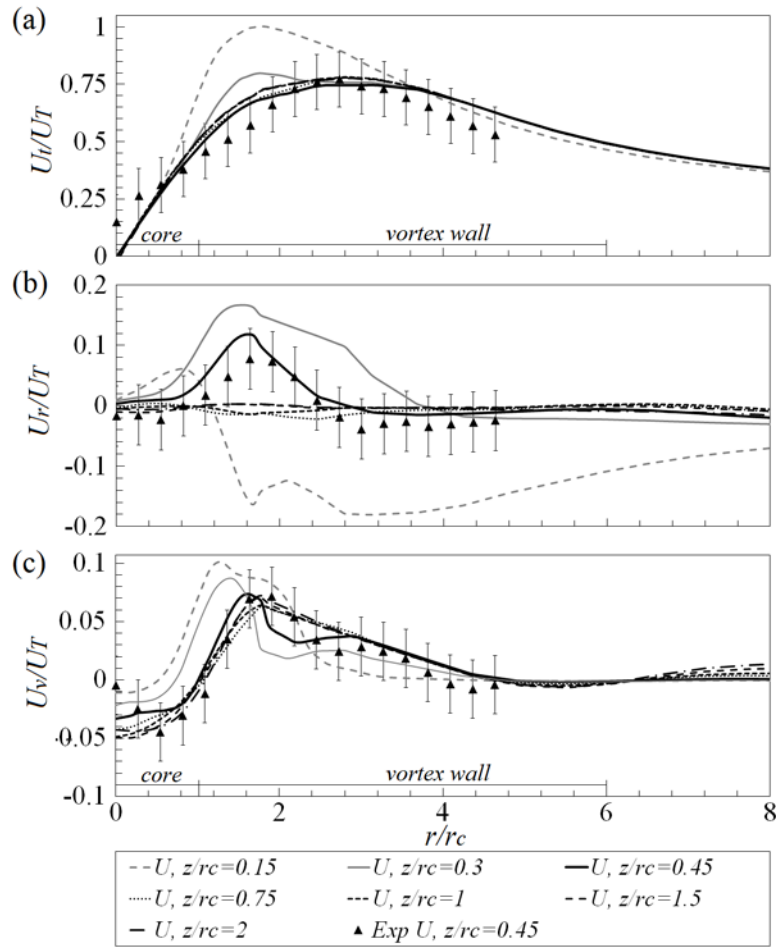
Figure 6: Horizontal profiles of time averaged velocity components at different elevation in comparison with experimental results (Exp) by Gillmeier et al. (2017).

Figure 6 shows the horizontal profiles of time averaged velocities extracted from the flow fields at the elevations of z/r_c=0.15, 0.3, 0.45, 0.75 1, 1.5 and 2. The experimental results by Gillmeier et al. (2017) were ensemble averages used as a comparison for the numerical simulation; data shown in the figure corresponds to the elevation of z/r_c=0.45 (where r_c is the core radius). The maximum tangential velocity of the vortex, U_T was 12.53 m/s and occurs at the radial distance, r_T of 1.82 (r/r_c=1.82) at the elevation of z/r_c=0.15; the velocity U_T was used as a characteristic velocity, as shown in figure 6(a).

The time per revolution of the vortex, t_r was calculated based on r_T and U_T, revealing the vortex to be approximately 0.1 seconds per revolution. The normalised radius of the core (r/r_c=1, where r_c= 0.11m) was calculated based on the averaged radial distance with respect to height of the layer with zero vertical velocity, (U_v/U_T=0) (as shown in figure 6(c)). The tangential velocity at r_c was U_t/U_T=0.48, and was used to mark the boundaries of the vortex wall spanning from approximately r/r_c=1 to 6 (as shown in figure 6(a)). As a result, the core at the centre of the vortex consists of low velocities, while high velocity magnitudes surround the core within the vortex wall.

In general, apart from the profile of z/r_c=0.15, the distribution of tangential velocity shows a similar trend and magnitude at all elevations. In figure 6(b), the profile at z/r_c=0.15 shows an outwards flow from the centre of the vortex to the radial distance of r/r_c=1.2 and then changes to inflow as the radial distance increases. Low magnitudes of radial velocity components were observed at higher elevations. Based on the profiles of vertical velocities in figure 6(c), a similar distribution can be observed at all elevations, with negative velocities at the centre of the vortex and increasing to maximum magnitude

290   between r/r_c=1.5 to 1.8. Some minor differences can be observed around the core region between
291   r/r_c=0 to 2, where the experimental results have the highest uncertainties. Overall, the predicted
292   velocity field matches that given by the physical results. However, both the numerical and physical
293   simulations are not without their limitations: accurately specifying inflow boundary conditions are
294   crucial for LES yet fraught potentially with difficulties (Yang, 2015), as very specific information on
295   turbulence is required to reproduce identical inflows, e.g., turbulence intensity, stochastically varying
296   turbulent length scales, and power spectrums of turbulent etc. The effects of sub-grid scale (SGS)
297   modelling is also considered to be a potential source of uncertainty since SGS motions inevitably
298   requires unrealistically fine cells at all regions even locations far away from the vortex structure.
299   Notwithstanding these limitations, the numerical results presented in the paper are within the range
300   of experimental uncertainty and considered suitable for the purposes of this work.

301   **4 RESULTS FOR DEBRIS FLIGHT**

302   The results for the simulation of debris flight using the flow field outlined in section 3.2 are presented
303   in this section. In all cases, the results have been normalized with the parameters of U_T, r_c and t_r as
304   appropriate. Debris group A, B1, B2, B3 and C (presented in table 1) were simulated at 50 different
305   time instances respectively; the release times were chosen at every quarter revolution of the vortex,
306   (t_r ≈0.025s). A total of 2250 individual debris groups were released from 9 different locations in the
307   flow; 5 locations within the core of the vortex at r/r_c=0, 0.25, 0.5, 0.75 and 4 locations away from the
308   core at r/r_c=1.5, 2, 2.5 and 3. Results from the simulation of debris group B1, B2 and B3 with identical
309   Tachikawa number of K=1.2 were compared for the aerodynamic similarity in section 4.1, while
310   section 4.2 investigates the behaviour of debris with varying Tachikawa number of K=2.5, 1.2 and 0.6
311   for debris group A, B1 and C respectively.

312   **4.1 RESULTS FOR DEBRIS B1, B2 AND B3 (K =1.2)**

313   The distribution of flight duration of all released debris are shown in figure 7 and expressed in terms
314   of the flight duration of each individual debris, t_d, normalized by the revolution of the vortex, t_r. The
315   flight duration was calculated based on the total airtime of debris from initialization to the impact on
316   the ground surface, where the maximum and minimum flight durations are represented by the
317   whiskers on the box plots. It can be observed that all 3 debris types show similar interquartile range
318   with positive skew; the mean flight duration (denoted by a "x") was approximately t_d/t_r ≈4 in all cases.
319   Debris that were not initialized or had a flight duration of less than a single revolution,(i.e., t_d/t_r <1)
320   were not considered as wind-borne in the current analysis; as a result, the total number of wind-borne
321   debris for debris group B1, B2 and B3 were 90, 82 and 86 respectively (20%, 18% and 19% for debris
322   group B1, B2 and B3 respectively). The low percentage of windborne debris were not too surprising
323   as this study focuses only on the wind-borne behaviour in a stationary tornado, where the translation
324   effects of the tornado were ignored. However, it is worth nothing that the translational movement of
325   a naturally occurring tornado could potentially result in higher percentage of debris becoming wind-
326   borne; several researches (Kosiba et al., 2014; Matsui et al., 2008; Phuc et al., 2012)have been carried
327   out where the translating speed of tornado ranges from 0.05 U_T to 0.7 U_T.

328   Figure 8 illustrates the plan view of the trajectories of wind-borne debris for debris group B1, B2 and
329   B3 that were initialized from the locations of r/r_c=0.5, 0.75, 1, 1.5 and 2. Data pertaining to the
330   locations r/r_c=0, 0.25, 2.5 and 3 are not shown since debris flight initialized from these locations was
331   infrequent, largely due to the downwards flow at the centre of the vortex region (r/rc=0 and 0.25) and
332   the absence of updraft flow at regions further from the core (r/rc=2.5 and 3). In general, the
333   trajectories of all debris from group B show a very similar path distribution at all locations, although
334   debris initialized from the location r/r_c=0.5 tends to show a greater degree of variation in trajectory.
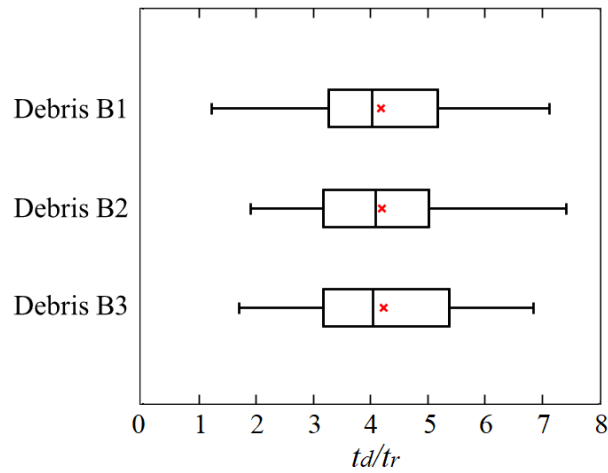
Figure 7: The distribution of flight duration of debris group B1, B2 and B3

The results from the experimental research conducted by Bourriez et al. (2017) were used as a comparison. The experimental study investigates the flight behaviour and motion of wind-borne debris in the tornado-like vortex at the swirl ratio of S=0.7. The debris used in the experiments were spherical polystyrene beads with varying diameter of 1.5 – 1.7 mm and densities of 24-28 kg/m^3, and corresponds to debris group B1 used in the simulation. The motion of the debris were tracked using the 3D-PTV technique (Maas et al., 1993; Malik et al., 1993). Two high speed digital cameras (Sony NEX-FS700RH) were positioned in the simulator and setup to record videos at 480 fps with the resolution of 1920 x 1080 pixels (confines of the tracking window not specified). Variations in results were found due to the relatively inconsistent size of the debris used, and the considerable changes on the local field of the vortex due to the wandering motion or turbulent fluctuations. Figure 9 shows the comparison of debris trajectories from numerical simulation and experimental results. The locations of r/r_c=1 and 2 corresponds to the closest release position from the experiments at r/r_c≈0.9 (100mm) and r/r_c≈1.8 (200mm).

The trajectories of the wind-borne debris were represented in black solid lines for the results from numerical simulation and the grey lines from the experiments while the red solid lines represents the mean trajectory of the numerical simulation and red dashed lines represents the mean trajectory of the experimental results.

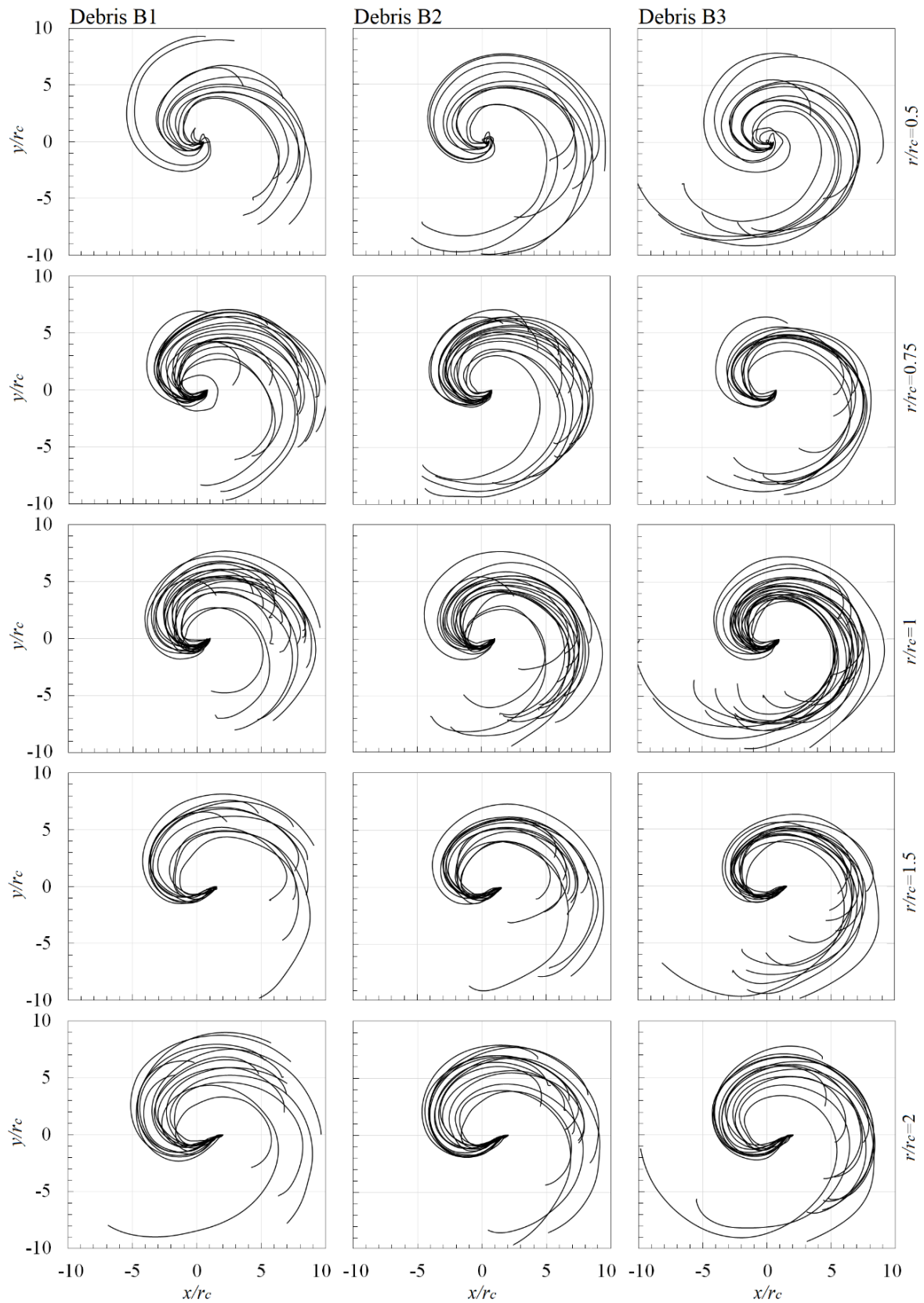Debris B1   Debris B2   Debris B3

$r/r_c=0.5$

$r/r_c=0.75$

$r/r_c=1$

$r/r_c=1.5$

$r/r_c=2$

y/r_c

x/r_c

354

Figure 8: Plan view of debris trajectories at the locations of r/r_c=0.5, 0.75, 1, 1.5 and 2 for debris group B1, B2 and B3.

357 All three debris groups predicted similar distributions of debris trajectories at both release positions,
358 while the debris trajectories from the experimental results shows shorter trajectories in comparison
359 with the numerical simulation as debris left the tracking window and the entire trajectories were not
360 captured. Both the numerical and experimental results corresponds well (considering the uncertainty
361 associated with the results) at the location $r/r_c=1$ with the overlapping trajectory path of
362 approximately 78%; while at the location $r/r_c=2$, the overlapping region was lower at approximately
363 61%; the numerical simulation predicted trajectories that were closer to the vortex core while the
364 experiment shows trajectories that were further from the core. The mean trajectories of both the
365 experiments and numerical simulations shows very similar curvature with the distance of
366 approximately r/rc=0.4 apart; this is likely due to the larger variation in the trajectory paths from the
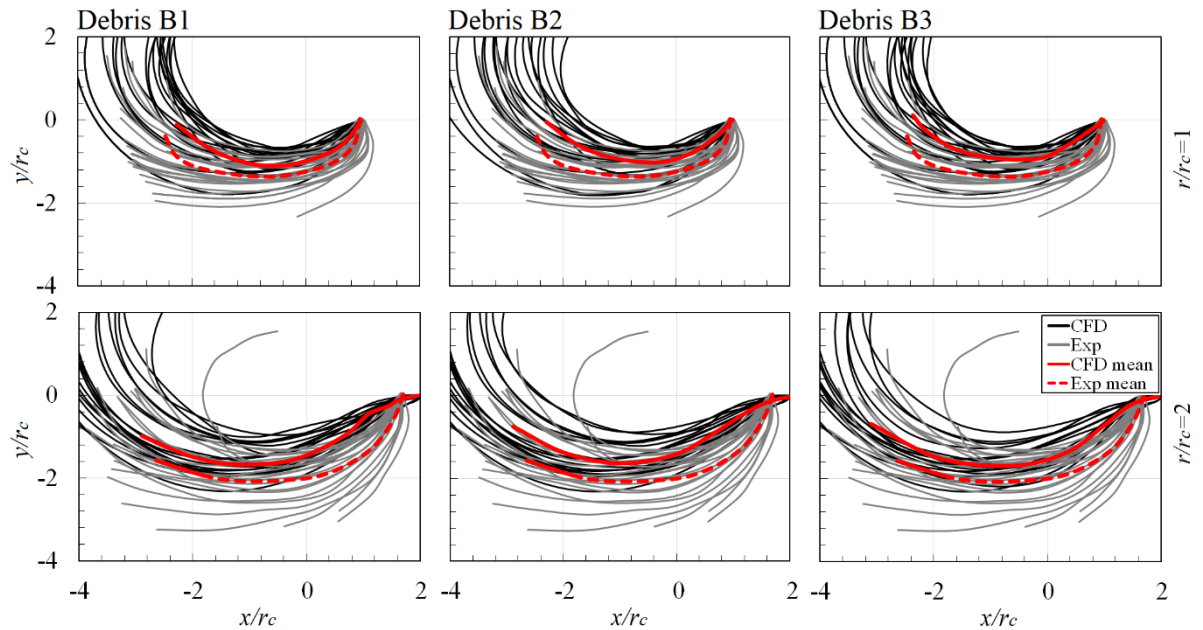367 experiments, caused by the turbulent fluctuation in the local field.

368

369 *Figure 9: A close-up view of debris trajectories at the locations of r/r$_c$=1 and 2 for debris group B1, B2 and B3 in*
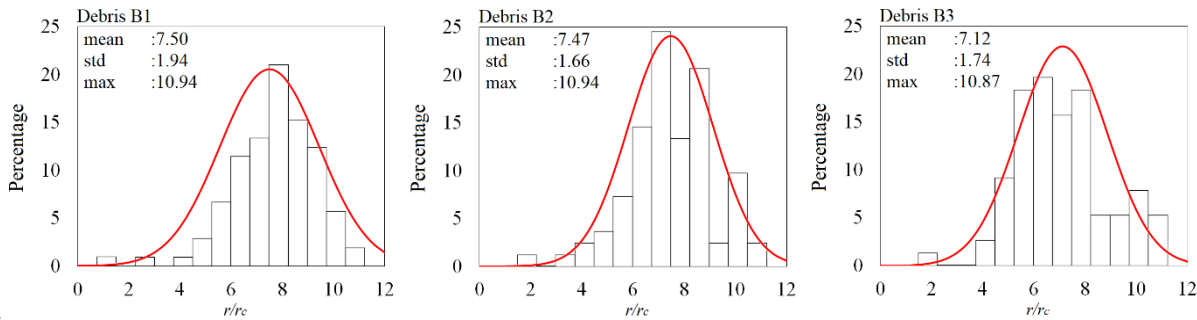370 *comparison with experimental data from Bourriez et. al (2017).*

371

372 *Figure 10: The distribution of impact radius of all released debris based on debris group, with mean, standard*
373 *deviation and maximum values.*

374 In figure 10, the bar chart shows the distribution of impact radius while the curve (red line)
375 corresponds to the normal distribution of all wind-borne debris, expressed in terms of the percentage
376 of occurrence against the impact radius. The distance between the impact locations and the centre of
377 the vortex was expressed as the impact radius as this provides a measurement of damage range for
378 the tornado-like vortex, while the percentage was calculated based on the number of occurrence for

379 wind-borne debris that impacts at that respective radial distance. The mean impact radius for debris
380 group B1, B2, and B3 were 7.5, 7.5 and 7.1 respectively. Due to high magnitudes of velocity
381 components between r/r_c=0 to 3, a sparse distribution of debris impact was observed around that
382 region. A clustered distribution of debris impact can be seen around the edge of the vortex walls that
383 is further away from the core (r/r_c > 6), where velocity magnitudes were low.

384 The aerodynamic similarity of debris group B1, B2 and B3 was examined. Understandably, all 3 debris
385 groups were shown to exhibit the propensity to travel with very similar flight duration and trajectories
386 due to the identical value of Tachikawa number. In general, the prediction of debris trajectories
387 corresponds well for both the numerical simulation and experiments results; however, it should be
388 pointed out that debris were assumed to be one-way coupled and the motion of debris were also
389 assumed with no rotation in a highly swirling flow, which may result in some difference in overall
390 trajectories between numerical and physical simulation. We also note the lack of turbulence data
391 associated with the physical measurements results in an uncertainty of the flow simulation in this
392 region. Notwithstanding this the numerical simulation are consistent with the physical data and able
393 to capture the entire flight duration from initialization to the impact on the ground. Furthermore, the
394 numerical simulations provide a better understanding of the impact distribution and extend the
395 results of the physical simulation.

396 **4.2 RESULTS FOR DEBRIS A, B1 AND C (K = 2.5, 1.2 AND 0.6 RESPECTIVELY)**

397 In this section, the behaviour of wind-borne debris in tornado-like vortex with varying Tachikawa
398 number (0.6 – 2.5) was studied. The distribution of flight duration for all released debris are shown in
399 figure 11, expressed in terms of the flight duration of each individual debris, t_d, normalized by the
400 revolution of the vortex, t_r. The flight duration was calculated based on the total airtime of debris from
401 initialization to the impact on the ground surface, where the maximum and minimum flight durations
402 are represented by the whiskers on the box plots. Debris that were not initialized or had a flight
403 duration of less than a single revolution, t_d/t_r <1 were not considered as wind-borne. As a result, the
404 total number of wind-borne debris for debris group A, B1 and C was 122, 90 and 54 respectively (27%,
405 20% and 12% for debris group A, B1 and C respectively). The Tachikawa number is a ratio of
406 aerodynamic forces relative to gravitational force of a wind-borne debris, therefore, light debris (low
407 mass) with high values of K will have the tendency to stay airborne for longer. Hence, the mean flight
408 duration (red "x") for all 3 debris groups were considerably different; the smaller and lighter debris A
409 has significantly longer flight duration than the heavier and larger debris C. The mean flight duration
410 for debris group A, B1 and C were t_d/t_r =5.49, 4.19 and 2.79 respectively.
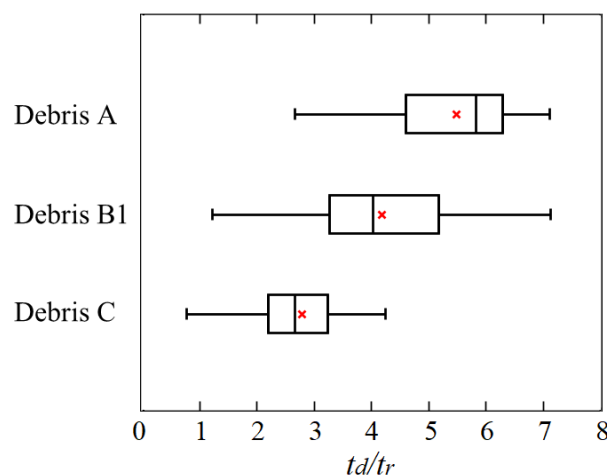

411

412 *Figure 11: The distribution of flight duration of debris group A, B1 and C.*

413   Figure 12(a) shows the percentage of wind-borne debris that were initialized by the vortex at different
414   radial positions. The percentage was calculated based on the number of debris that were initialized
415   by the vortex at that position with respect to the total number of wind-borne debris (122, 90 and 54
416   debris for debris group A, B1 and C respectively). Hence, at the location r/r_c=1, 30 individual debris
417   particles from group A were initialized yielding 24%, while 13 individual debris of debris group C were
418   initialized yielding 24%. Figure 12(b) shows the horizontal profiles of tangential, radial and vertical
419   velocity components that corresponds to the debris release positions. The scales of the normalized
420   vertical velocity are shown on the left vertical axis while the normalized tangential and radial velocity
421   are shown on the right vertical axis. This was done to highlight the distribution of vertical profile
422   without being overshadowed by the high magnitudes of tangential velocity. As discussed earlier, the
423   centre of the vortex primarily consists of downwards flow, while maximum magnitude of updraft flow
424   can be found around the vortex core region, r/r_c=1. A relatively high magnitude of tangential velocity
425   is present at the region r/r_c>1. Based on the figure, it can be observed that the percentage distribution
426   of debris initialization based on the position shows a correlation with the vertical velocity profile.
427   Furthermore, all three debris groups illustrate similar trends with the highest percentage at the core
428   radius, r/r_c=1 despite the difference in total number of debris considered as wind-borne. Regions
429   further away at r/r_c=2.5 and r/r_c=3, and around the centre of the vortex at r/r_c=0 and r/r_c=0.25 were
430   observed to have a very low possibility of flight initiation by the flow despite the high magnitudes of
431   tangential and radial velocities. The increase of vertical flow from r/r_c=0.5 to r/r_c=2 resulted in the
432   increase in the percentage of debris initialization, where debris that were positioned around this
433   region were approximately 10% more likely to be initialized. This is due to the upwards lift produced
434   by the vertical velocity that provides the elevation for debris to become wind-borne. A small number
435   of particles appear to have become windborne for debris A and B at r/r_c=0. This is due to the wandering
436   motion of the vortex, where the core shifted approximately r/r_c=0.18 from the centre axis. Although
437   the shift is not significant, the radial outflow at the centre in addition with the absence of downward
438   flow provided sufficient condition for debris to become wind-borne.

439   Figure 13 illustrates the plan view of the trajectories of all wind-borne debris for debris group A, B1,
440   and C that were initialized from the position of r/r_c=0.5, 0.75, 1, 1.5 and 2 to the impact on the ground
441   surface. The positions of r/r_c=0, 0.25, 2.5 and 3 are not shown as debris initialized from those locations
442   was infrequent. The smaller debris (group A) were observed to have high variation in debris
443   trajectories at all positions and the longest average flight duration. In this case, the debris were
444   observed to circulate around the vortex core, resulting in long and scattered trajectories. On the
445   contrary, the trajectories for the larger debris group C shows lower curvature and does not have the
446   tendency to circulate around the vortex. In general, the distribution of trajectories for each respective
447   debris group shows similar variation at every position.

448   In figure 14, the bar chart shows the distribution of impact radius while the curve (red line)
449   corresponds to the normal distribution of all wind-borne debris, expressed in terms of the percentage
450   of occurrence against the impact radius. The percentage was calculated based on the number of
451   occurrences of wind-borne debris that impacted at that respective radial distance. A different range
452   of impact radii were observed for groups A, B1 and C: debris A shows the shortest mean impact radius
453   of r/r_c ~ 7.0, whilst debris C has the greatest impact radius of r/r_c ~9.0. Concurrently, debris C exhibited
454   the highest impact potential with a maximum value of r/r_c= ~12.0, whereas debris A and B shows
455   comparable maximum impact radii of r/r_c ~11.0. The normal distribution suggests similar variation for
456   all debris, with the standard deviation for each group ~2.0. Although the smaller and lighter debris A
457   has longer flight duration, it does not impact at greater radial distance from the vortex; this
458   phenomenon will be discussed and shown in figure 15.

459 Figure 15 shows the total flight duration of each individual wind-borne debris from initialization to the
460 impact on the ground against the radial distance from the centre of the vortex throughout the flight.
461 Thus, providing an insight to the debris trajectories in relation to the regions of the vortex whilst also
462 characterising the behaviour of different debris groups. All debris shows a reduction in radial distance
463 once initialized, indicating the tendency to travel towards the centre before for values of $t_d/t_r < 0.4$.
464 For debris group A, the radial distance for the debris were observed to increase rapidly away from the
465 centre after the flight time of $t_d/t_r > 0.4$; while some debris were ejected outwards with the radial
466 distance of more than $r/r_c = 8$, the majority of the debris circulates around the region between $r/r_c=6$
467 to 8 after the flight duration of $t_d/t_r = 2$. . Towards the end of the flight duration, a decrease in radial
468 distance was observed as the debris were drawn towards the vortex due to the radial inflow, as shown
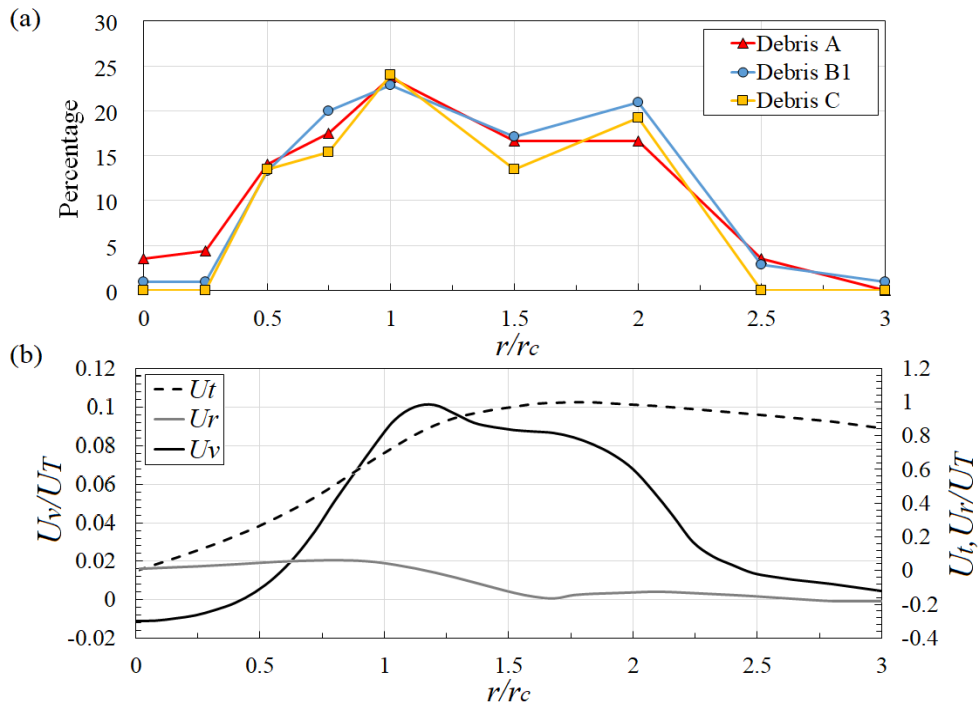469 in figure 16.

470

471 *Figure 12: (a) The percentage distribution of all wind-borne debris at the position of r/r_c=0, 0.25, 0.5, 0.75, 1,*
472 *1.5 2, 2.5 and 3. (b) The horizontal profiles of tangential, radial and vertical velocities of the tornado-like vortex*
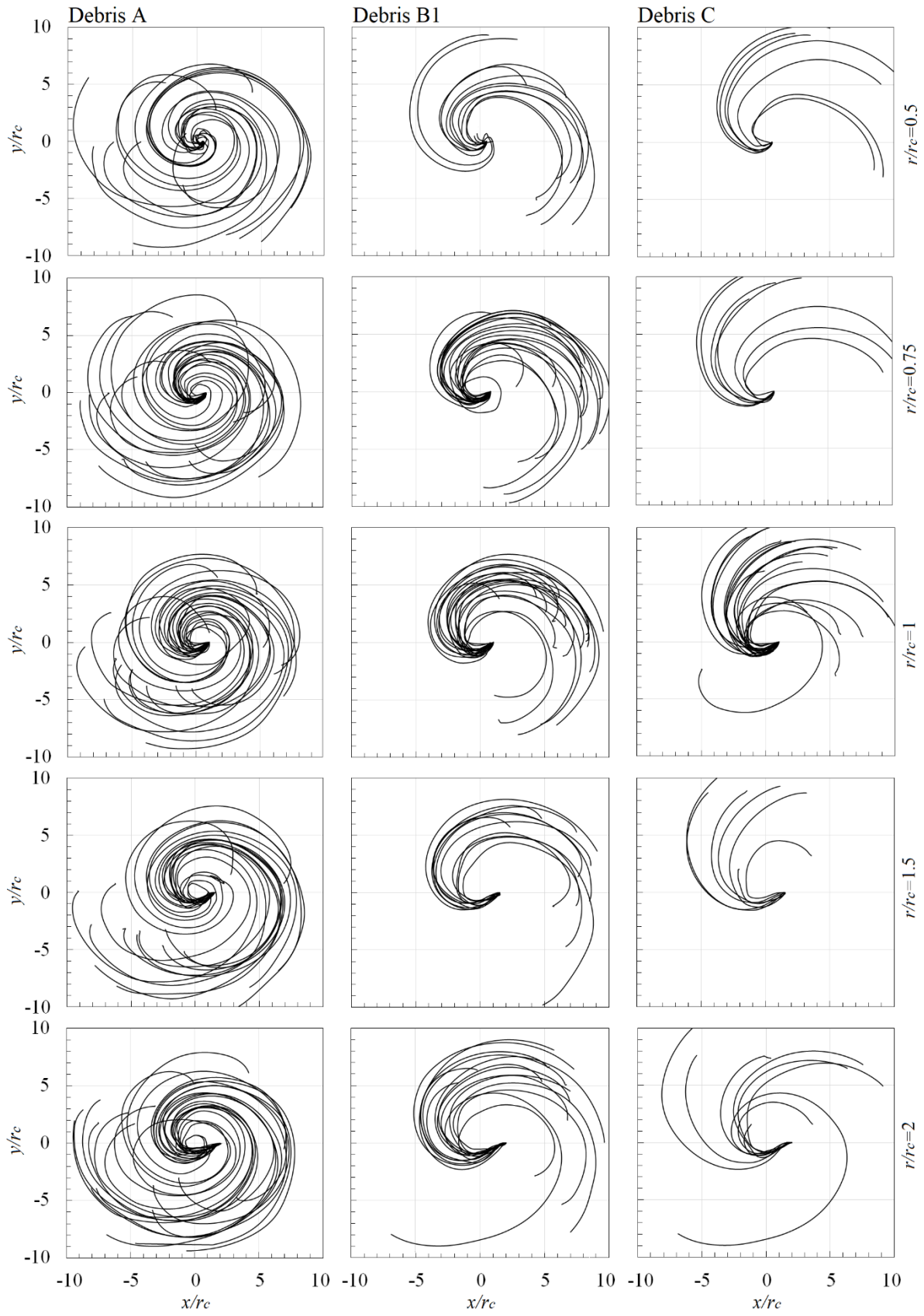473 *at the elevation of z/r_c=0.015.*

474

Figure 13: Plan view of debris trajectories at the locations of r/rc=0.5, 0.75, 1, 1.5 and 2 for debris group A, B1 and C.
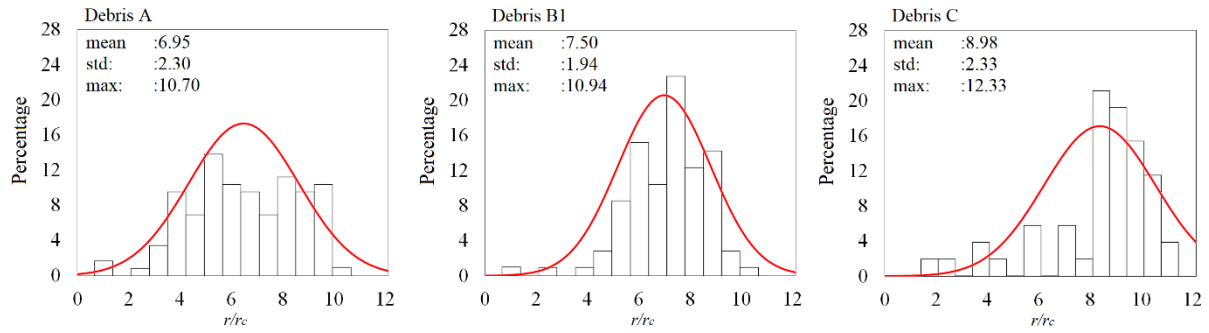
Figure 14: The distribution of impact radius of all released debris based on debris group, with mean, standard deviation and maximum values.

In general, the debris group A has approximately 60% of the flight duration around the vortex walls regions. On the contrary, the radial distance of debris group C were observed to constantly increase throughout the flight duration due to the inertia of the debris, travelling further away from the centre until the impact on the ground. The trajectories of debris group B exhibited a mixture of behaviours with some particles travelling beyond the vortex wall whilst others circulated close to walls.
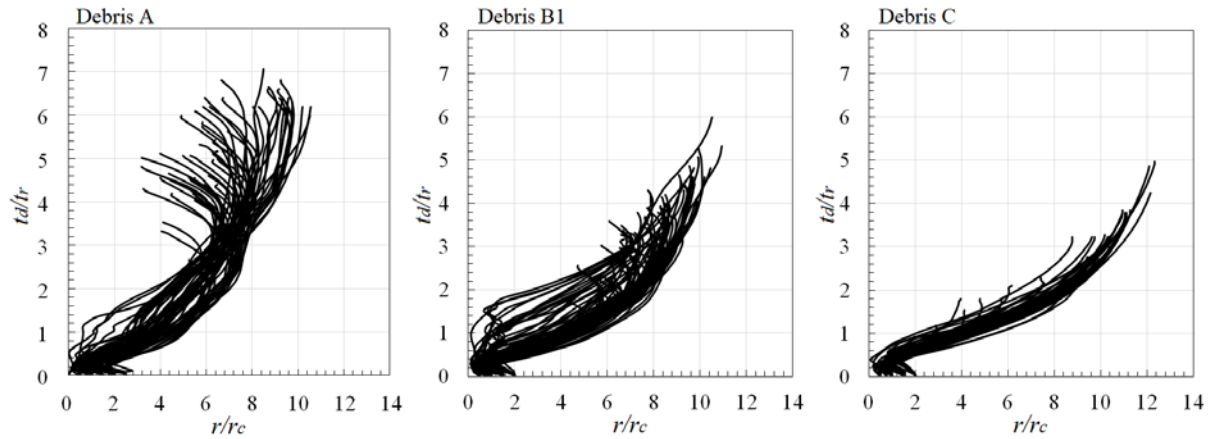

Figure 15: The flight duration of wind-borne debris against the radial distance from the centre of the vortex for debris group A, B1 and C.
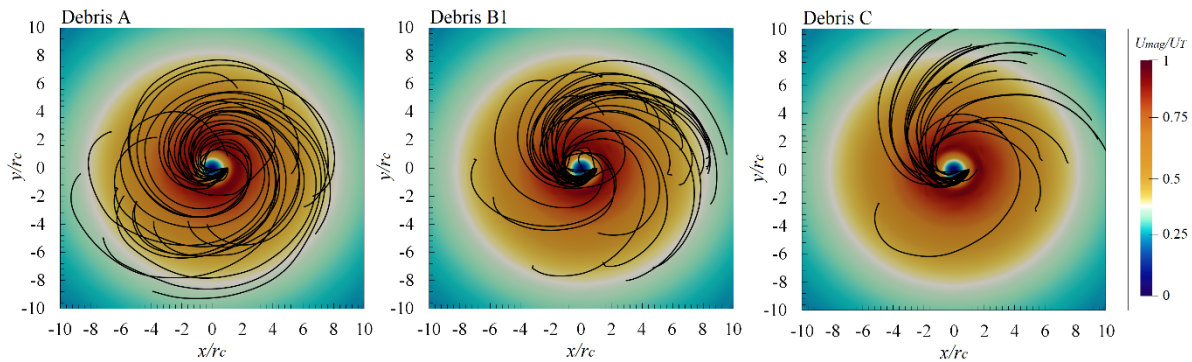
Figure 16: The top view of debris trajectories at the location r/r_c=1 with the contours of averaged velocity magnitude for debris group A, B1 and C.

The plan view of the trajectories of the debris initialized from the position r/r_c=1 with contours of normalized tangential velocity shown in figure 16. The red contours in figure 16 indicates the vortex walls. As discussed previously, the trajectories of debris group A are observed to circulate within the vortex wall between r/r_c= 1 to 6 with a tendency to be drawn back towards the core at end of the

495   flight duration. However, for debris group C it is clear that the vast majority of debris are ejected away
496   from the centre and out of the vortex walls.

497   **5. CONCLUSIONS**

498   The objective of this present research was to investigate the flight behaviour of different groups of
499   debris in a tornado-like wind field. Hence, large eddy simulations were undertaken for a tornado-like
500   vortex with a swirl ratio of 0.7. Acknowledging the uncertainty associated with the data, the numerical
501   simulations agree well with previous experimental research and provide a greater insight into the flow
502   field. The following conclusions can be made:

503   • The tornado-like vortex consists of two main features, a core and thick vortex wall around the
504   core. The vortex wall consists of high velocity magnitudes where the maximum velocity
505   components occurs around the near ground region.
506   • The aerodynamic behaviour for three groups with the same Tachikawa number (B1, B2 and
507   B3) shows very similar flight behaviour and trajectories. All three debris groups exhibit a mean
508   flight duration of $t_d/t_r \approx 4$ with an impact radius of $r/r_c \sim 7.5$.
509   • The aerodynamic behaviour for three groups with varying Tachikawa numbers (A, B1 and C)
510   demonstrated that debris group with a lower mass (A) has the highest percentage of wind-
511   borne particles (~27%) compared to 20% and 12% for debris group B1 and C respectively.
512   Group A also had a considerably longer flight duration ($t_d/t_r \sim 6.0$), than groups B and C with
513       $t_d/t_r \sim 4.0$ and 3.0 respectively. During debris initializing stage, the debris positioned at the
514   radial location of $r/r_c=1$ had the highest possibility of becoming wind-borne, whereas debris
515   positioned around the regions within the core at $r/r_c=0$ and 0.25 and at regions where $r/r_c >$
516   2.0 were less likely to be initialized. This was due to the higher vertical velocities around $r/r_c =$
517   1 which appear to be key to flight initiation.
518   • The distribution of trajectories for debris group A were found to be scattered with high
519   variation but low average impact range of $r/r_c= 7.0$, whilst debris group C has trajectories with
520   a lower curvature but greater high radius ($r/r_c \sim 9.0$). Further analysis of the flight duration
521   indicated that debris group A had the tendency to circulate within the regions of vortex walls
522   with consistent radial distance from the centre, whereas for group C the radial distance was
523   observed to constantly increase until the particles impacted on the ground.
524   • Low mass debris with high values of K were prone to travel for longer flight duration but as
525   indicated above, tended to be trapped within the vortex walls. This has important implications
526   when considering the wind loading arising from wind borne debris as a result of tornadic
527   activity.

528   The flow field of the tornado-like vortex and the flight behaviour of different debris groups were
529   discussed in detail. It is worth noting that current study only considers the flow field of the vortex at
530   S=0.7. Different swirl ratios have the potential to result in different flow characteristics and those
531   would affect the overall behaviour of wind-borne trajectory. Further, the flight characteristics of
532   debris were assumed with no rotation, which might be considered less realistic in a highly swirling
533   vortex flow field when the rotation of debris generates lift, which would lead to a different interaction
534   between the fluid and debris. It is also worth noting that this work has simulated the flow assuming
535   one single definition of aspect ratio, but as indicated by Gillmeier et al. (2019) and Gairola and
536   Bitsuamlak (2019), this may be an important area which has hitherto largely been neglected.
537   Notwithstanding this, this research shows the flight behaviour of different debris groups and their
538   corresponding impact range and thus enables the potential dangers associated with flying debris in
539   tornadoes to be evaluated.

Reference

[1]. Alexander, C.R., Wurman, J., 2005. The 30 May 1998 Spencer, South Dakota, Storm. Part I: The Structural Evolution and Environment of the Tornadoes," AMS Monthly Weather Review, v. 133, 72-96.

[2]. Baker, C. J., 2007. The debris flight equations. Journal of Wind Engineering and Industrial Aerodynamics 95(5):329-353.

[3]. Baker, C.J., Sterling, M., 2017. Modelling wind fields and debris flight in tornadoes, J. Wind Eng. and Ind. Aerody., 168, 312-321.

[4]. Bourriez, F., Sterling, M., Baker, C.J., 2017. Physically modelling windborne debris in tornado-like flow, 9th Asia-Pacific Conference on Wind Engineering, Auckland, New Zealand, 2017.

[5]. Courant, R., Friedrichs, K., Lewy, H., 1928. Über die partiellen Differenzengleichungen der mathematischen Physik, Mathematische Annalen (in German), 100 (1): 32–74.

[6]. Darrow, M., 2019. Day 4-8 Severe Weather Outlook Issued on Feb 28, 2019. Norman, Oklahoma: Storm Prediction Center. Retrieved from https://www.spc.noaa.gov/products/exper/day4-8/archive/2019/day4-8_20190228.html

[7]. English, E. C., Holmes, J. D., 2005. Non-dimensional solutions for trajectories of wind-driven compact ob-jects, Proceedings of The Fourth European and African Conference on Wind Engineering.

[8]. Evans, S., 2019. U.S. Severe weather in May to drive $2 Billion or greater financial impact on: AON. Retrieved from https://www.artemis.bm/news/u-s-severe-weather-in-may-to-drive-2bn-or-greater-financial-impact-aon/

[9]. Gairola, A., Bitsuamlak, G., 2019. Numerical tornado modelling for common interpretation of experimental simulators. Journal of Wind Engineering and Industrial Aerodynamics, Volume 186, pages 32-48.

[10]. Gillmeier, S., Hemida, H. and Sterling, M., 2016. An analysis of the influence of a tornado generators geometry on the flow field. 8th International Colloquium on Bluff Body Aerodynamics and Applications June 7 – 11.

[11]. Gillmeier, S., Sterling, M., Baker, C.J. and Hemida, H., 2017. A reflection on analytical vortex models used to model tornado-like flow fields. International Workshop on Physical Modelling of Flow and Dispersion Phenomena Dynamics of Urban and Coastal Atmosphere.

[12]. Gillmeier, S., Sterling, M., and Hemida, H (2019). Simulating Tornado-Like Flows – the Effect of the Simulator's Geometry. Meccanica. Vol. 54, No. 15, 2385-2398, https://doi.org/10.1007/s11012-019-01082-4.

[13]. Hangan, H. and Kim, J.D., 2006. Numerical simulation of Tornado Vortices. The 4th International Symposium on Computational Wind Engineering, Yokohama.

[14]. Hangan, H. and Kim, J.D., 2008. Swirl ratio effects on tornado vortices in relation to the Fujita scale.WindStruct.11, 291–302.

[15]. Harms, Associate Writer Nicole. (2019, February 17). Why Are Tornadoes So Terrifying? Retrieved from https://www.thoughtco.com/tornado-safety-overview-3444293

[16]. Holmes, J. D., Baker, C. J., Tamura ,Y., 2006. Short note Tachikawa number: A proposal, Journal of Wind Engineering and Industrial Aerodynamics 94, 41-47.

585 [17]. Holmes, J. D., 2004. Trajectories of spheres in strong winds with application to wind-borne
586   debris, Journal of Wind Engineering and Industrial Aerodynamics 92, 9-22.
587 [18]. Holmes, J. D., English, E. C., Letchford, C., 2004. Aerodynamic forces and moments on cubes
588   and flat plates, with applications to wind-borne debris, Summary Papers of the 5th
589   International Colloquium on Bluff Body Aerodynamics and Applications, 103-106.
590 [19]. Howells, P.C., Rotunno, R., Smith, R.R., 1988. A comparative study of atmospheric and
591   laboratory analogue numerical tornado-vortex models. Quarterly Journal of Royal
592   Meteorological Society 114, 801–822
593 [20]. ICEM, C., 2012. ver. 14.0. ANSYS Inc., Southpointe, 275.
594 [21]. Ishihara, T. and Liu, Z.Q., 2014. Numerical study on dynamics of a tornado-like vortex with
595   touching down by using the LES turbulence model. Wind and Structures, Vol, 19, No. 1 000-
596   000.
597 [22]. Ishihara, T., Oh, S. and Tokuyama, Y., 2011. Numerical study on flow fields of tornado-like
598   vortices using the LES turbulence model. Journal of Wind engineering and Industrial
599   Aerodynamics 99, 239–248.
600 [23]. Kosiba, K. A., Robinson, P., Chan, P. W., & Wurman, J. (2014). Wind Field of a Non mesocyclone
601   Anti cyclonic Tornado Crossing the Hong Kong International Airport. Advances in Meteorology,
602   1-7.
603 [24]. Kuai, L., Haan, F.L., Gallus, W.A. and Sarkar, P.P., 2008. CFD simulations of the flow field of a
604   laboratory-simulated tornado for parameter sensitivity studies and comparison with field
605   measurements. Wind and Structures. 11, 1-22.
606 [25]. Kuai, L., Haan, F.L., Gallus, W.A. and Sarkar, P.P., 2008. CFD simulations of the flow field of a
607   laboratory-simulated tornado for parameter sensitivity studies and comparison with field
608   measurements. Wind and Structures. 11, 1-22.
609 [26]. Lewellen, D.C., Lewellen, W.S., 2007. Near-surface intensification of tornado vortices. Journal
610   of the Atmospheric Sciences 64, 2176–2194.
611 [27]. Lewellen, D.C., Lewellen, W.S., Xia, J., 1999. The influence of a local swirl ratio on tornado
612   intensification near the surface. Journal of the Atmospheric Sciences57, 527–544.
613 [28]. Lin, N., Holms J. D., Letchford, C. W., 2007. Trajectory of windborne debris and applications to
614   impact test-ing, J. Structural Eng. ASCE, 133(2), 274-282.
615 [29]. Liu, Z, Ishihara, T., 2015. Numerical study of turbulent flow fields and the similarity of tornado
616   vortices using large eddy simulations. Journal of Wind engineering and industrial
617   aerodynamics. 145, 42-60.
618 [30]. Maruyama, T., 2009. A Numerically Generated Tornado-like Vortex by Large Eddy Simulation,
619   Proceedings of Seventh Asia-Pacific Conference on Wind Engineering, Taipei Taiwan, 2009.8,
620   pp. 349-352.
621 [31]. Maruyama, T., 2011. Simulation of flying debris using a numerically generated tornado-like
622   vortex. J. Wind Eng. Ind. Aerod. 99, 249–256.
623 [32]. Maas H-G, Gruen A., Papantomiou D., 1993. Particle tracking velocimetry in three-dimensional
624   flows. Part I. Exp Fluid, 15:133–46.
625 [33]. Malik N.A., Dracos T., Papantomiou D., 1993. Particle tracking velocimetry in three-
626   dimensional flows. Part II. Exp Fluid, 15:279–94.
627 [34]. Matsui, M., Tamura, Y., Yoshida, A., 2008. Wind pressure distribution around cube in tornadic
628   flow and moving effects on tornadic flow, Proc. 20th National Symposium on Wind
629   Engineering, pp.319-324 (Japanese).
630 [35]. Matsui, M., Tamura,Y., 2009. Influence of swirl ratio and incident flow conditions on
631   generation of tornado-like vortex. In: Proceedings of the 5th European and African Conference
632   on Wind Engineering. CD-ROM.

633   [36]. Mitsuta, Y., Monji,N., 1984. Development of a laboratory simulator for small scale
634   atmospheric vortices. Nat. Disaster Sci.6, 43–54.
635   [37]. Monji, N., 1985. A laboratory investigation of the structure of multiple vortices. J. Meteorol.
636   Soc. Jpn. 63, 703–712.
637   [38]. Natarajan, D., 2011. Numerical Simulation of Tornado-like Vortices. (Unpublished doctoral
638   thesis). University of Western Ontario, Canada.
639   [39]. Nolan, D.S., Farrell, B.F., 1999. The structure and dynamics of tornado-like vortices. Journal of
640   the Atmospheric Sciences 56, 2908–2936.
641   [40]. OpenFOAM,   2019.   OpenFOAM: User   guide   version   7.   Retrieved   from
642   http://foam.sourceforge.net/docs/Guides-a4/OpenFOAMUserGuide-A4.pdf
643   [41]. Phuc, P.V., Nozu, T., Nozawa, K., Kikuchi, H., 2012. A Numerical Study of the Effects of Moving
644   Tornado-Like Vortex on a Cube. The Seventh International Colloquium on Bluff Body
645   Aerodynamics and Applications (BBAA7) Shanghai, China; September 2-6, 2012.
646   [42]. Putnam, A., 1961. Integrable form of droplet drag coefficient, ARS Jnl., 31, 1467.
647   [43]. Smagorinsky, J., 1963. General Circulation Experiments with the Primitive Equations. Monthly
648   Weather Review. 91 (3): 99–164.
649   [44]. Refan, Maryam & Hangan, Horia. (2018). Near surface experimental exploration of tornado
650   vortices. Journal of Wind Engineering and Industrial Aerodynamics. 175C.
651   [45]. Richards, P.J., Williams, N., Laing, B., McCarty, M., Pond, M., 2008. Numerical calculation of
652   the 3-dimensional motion of wind-borne debris, J. Wind Eng. and Ind. Aerody., 96, 2188-2202.
653   [46]. Tachikawa, M., 1983. Trajectories of flat plates in uniform flow with application to wind-
654   generated missiles, Journal of Wind Engineering and Industrial Aerodynamics 14, 443-453.
655   [47]. Tang, Z., Feng, C., Wu, L., Zuo, D., James, D.L. (2018) "Characteristics of tornado-like vortices
656   simulated in a large-scale ward-type simulator." Boundary-Layer Meteorology, 166, 327-350.
657   [48]. Tari, P.H., Gurka, R., Hangan,H., 2010. Experimental investigation of tornado-like Vortex
658   dynamics with swirl ratio: the mean and turbulent flow fields. J.Wind Eng.
659   Ind.Aerodyn.98,936–944.
660   [49]. Van Driest, E.R., 1956. Turbulent flow near a wall, J. Aeronaut. Sci., 23, No. 11, 1007-1011.
661   [50]. Wang, K,. and Letchford, C. W., 2003. Flying debris behaviour, 11th International Conference
662   on Wind Engineering, Lubbock, Texas Proceedings 2, 1663-1670.
663   [51]. Ward, N. B., 1972. The exploration of certain features of tornado dynamics using a laboratory
664   model. J. Atmos. Sci., 29, 1194-1204.
665   [52]. Watkins, S., Mousley, P.D., Hooper, J.D., 2002. Measurement of fluctuating flows using multi-
666   hole probes. Proceedings of the 9th International Congress of Sound and Vibration, Orlando,
667   Florida, USA, 8-11 July, International Institute of Acoustics and Vibration (IIAV).
668   [53]. Wilson, T., Rotunno, R., 1986. Numerical simulation of a laminar end-wall vortex and boundary
669   layer. Phys. Fluids 29, 3993–4005.
670   [54]. Wills, J. A. B., Lee, B. E., and Wyatt, T. A., 2002. A model of wind-borne debris damage, Journal
671   of Wind Engineering and Industrial Aerodynamics 90, 555-565.
672   [55]. Yang, Z, 2015 Large-eddy simulation: Pass, Present and the future. Chinese Journal of
673   Aeronautics, (2015), 28 (1): 11-24.